Shocked Quartz in Polymict Impact Breccia from the Upper Cretaceous Yallalie Impact Structure in Western Australia

Morgan A. Cox[1], Aaron J. Cavosie[1] , Ludovic Ferrière[2] , Nicholas E. Timms[1], Phil A. Bland[1], Katarina Miljković[1], Timmons M. Erickson[1, 3] and Brian Hess[4]

[1] *Space Science and Technology Centre, School of Earth and Planetary Sciences, Curtin University, Perth, WA 6102, Australia*

(morgan.cox@student.curtin.edu.au)

[2] *Natural History Museum, Burgring 7, A-1010 Vienna, Austria*

[3] *Jacobs- JETS, Astromaterials Research and Exploration Science Division, NASA Johnson Space Center, Houston, Texas, 77058, USA*

[4]*NASA Astrobiology Institute, Department of Geoscience, University of Wisconsin–Madison, Madison, Wisconsin 53706, USA*

ABSTRACT

Yallalie is a ~12 km diameter circular structure located ~200 km north of Perth, Australia. Previous studies have proposed that the buried structure is a complex impact crater based on geophysical data. Allochthonous breccia exposed near the structure has previously been interpreted as proximal impact ejecta, however no diagnostic indicators of shock metamorphism have been found. Here we report multiple (27) shocked quartz grains containing planar fractures (PFs) and planar deformation features (PDFs) in the breccia. The PFs occur in up to 5 sets per grain, while the PDFs occur in up to 4 sets per grain. Universal stage measurements of all 27 shocked quartz grains confirms that the planar microstructures occur in known crystallographic orientations in quartz corresponding to shock compression from 5 to 20 GPa. Proximity to the buried structure (~4 km) and occurrence of shocked quartz indicates that the breccia represents either primary or reworked ejecta. Ejecta distribution simulated using iSALE hydrocode predicts the same distribution of shock levels at the site as those found in the breccia, which supports a primary ejecta interpretation, although local reworking cannot be excluded. The Yallalie impact event is stratigraphically constrained to have occurred in the interval from 89.8-83.6 Ma based on the occurrence of Coniacian clasts in the breccia and undisturbed overlying Santonian to Campanian sedimentary rocks. Yallalie is thus the first confirmed Upper Cretaceous impact structure in Australia.

INTRODUCTION

Impact cratering is a widespread geological process throughout the solar system. The presence of shatter cones, shocked minerals, high-pressure phases, and geochemical evidence for the presence of meteoritic material (e.g., French 1998; French and Koeberl 2010) has thus far led to the confirmation of about 190 terrestrial impact craters to date (*Earth Impact Database*, 2018). Shock deformation microstructures in minerals form when the shock wave produced by hyper-velocity impact travels through target rocks (Stöffler and Langenhorst 1994 and references therein). Quartz is perhaps the most widely reported shocked mineral in terrestrial impactites. Shock microstructures in quartz such as planar fractures (PFs) and planar deformation features (PDFs) record shock pressures from 5-30 GPa and are readily identified using a petrographic microscope (e.g., Stöffler and Langenhorst 1994; Huffman and Reimold 1996; Ferrière and Osinski 2013). Here we report the first diagnostic evidence of shock deformation in quartz grains in allochthonous breccia from the Yallalie structure in Western Australia.

Regional Geology

The geology of the study area consists of Mesozoic sedimentary rocks, including sandstone, siltstone, shale, and limestone (chalk), of the Dandaragan Trough within the greater Perth Basin (Fig. 1). The Darling Fault lies ~10 km east of the previously proposed rim of the Yallalie structure (Dentith et al. 1999), with the Archean Yilgarn Craton located on the eastern side of the fault (Fig. 2). The Dandaragan Trough is an asymmetrical graben that contains sedimentary successions up to 15 km thick (Harris 1994; Mory and Iasky 1996; Timms et al. 2015; Olierook et al. 2015). The trough is the deepest part of the Perth Basin; sedimentary rocks that lie within it were deposited in intracontinental rifts during the breakup of Gondwana and development of a passive margin (Harris 1994; Sircombe and Freeman 1999; Song and Cawood 2000; Veevers et al. 2005).

The Yallalie Structure

The Yallalie structure was first described in an impact context in a 1992 Meteoritical Society abstract (Dentith et al. 1992). Seismic surveys conducted across the structure by Ampol Exploration Ltd. in 1988 and 1990 showed a zone of disruption that extends to ~1500 m below the surface, with an abrupt contact between the structure and overlying sedimentary units (Dentith et al. 1999; Hawke 2004; Hawke et al. 2006). A 3 to 4 km wide central uplift was identified by Dentith et al. (1999) from seismic data. A small positive gravity anomaly of 30 gu (3 mGal) was described by Dentith et al. (1999) based on a north-south transect across the center of the Yallalie structure, and attributed to uplifted bedrock. Airborne magnetic surveys reveal a 12 km diameter circular feature, consisting of concentric positive magnetic anomalies, further suggesting the presence of a complex structure (Hawke et al. 2006). Two petroleum exploration wells, Cypress Hill-1 (Higgins 1988) and Yalallie-1 (Economo 1991), were drilled within the structure (Fig. 2). Cypress Hill-1 (30°27'51" S, 115°48'42" E) was drilled in 1988 and penetrated 990 m along the southeast rim, intersecting a rotated fault block. Yallalie-1 (30°20'40" S, 115°46'16" E) was drilled in 1990 and penetrated 3322 m into the center of the structure. In both cases, the wells were not continuously cored, therefore geological contacts were interpreted from wireline log data (Bevan 2012).

The Yallalie structure is thus buried below ~100-300 m of undisturbed sediment, which includes thin layers of lacustrine sediment, laterite, and recent aeolian sand (Dentith et al. 1999; Hawke et al. 2006). The target rocks are all sedimentary, and, in general, consist of poorly sorted, interbedded, marine and fluvial sandstone, siltstone, shale, chalk, and glauconitic sandstone (greensand) (Belford 1959; Playford et al. 1976; Moray and Iasky 1996; Timms et al. 2015). Rocks affected by the proposed impact event include the Jurassic Yarragadee Formation (below 320 m current depth), which is overlain by the Cretaceous Parmelia Formation (Warnbro Group), and Leederville Formation (Coolyena Group), respectively (Dentith et al. 1999; Olierook et al. 2015).

Allochthonous breccia, informally named the “Mungedar Breccia” (Bevan 2012), outcrops 4 km west of the rim of the buried structure (Fig. 2), and is the only exposed geological unit known that has been interpreted to have originated from the proposed

Yallalie impact event (e.g., Dentith et al. 1999). The breccia sits unconformably on Upper Cretaceous siliciclastic rocks, and no other comparable anomalous breccia occurrences are known from elsewhere in the Perth Basin (Dentith et al. 1999; Bevan et al. 2004; Bevan 2012). The breccia contains up to meter-scale blocks of sedimentary rocks, and has a maximum thickness estimated at ~30 m. The breccia was previously interpreted as an allochthonous polymictic breccia that formed from material ejected during the proposed Yallalie impact event (Dentith et al. 1999).

Fractured quartz grains from cuttings in the Yallalie-1 borehole (Dentith et al. 1999) and in exposed Mungedar Breccia (Bevan, 2012) have been described previously, however, none of the planar microstructures in those grains were indexed by universal stage. Diagnostic evidence of shock microstructures has thus far not been documented in any materials associated with the Yallalie structure. Despite the convincing geophysical anomalies and reports of fractured quartz grains, until now no evidence of shock deformation has been reported that could substantiate an impact origin of the Yallalie structure to be confirmed.

The relative age of the structure is constrained primarily by stratigraphic relations interpreted from cuttings in the Yallalie-1 core, along with tentative correlation of clasts found within the allochthonous breccia exposed in the area (Dentith et al. 1999). The depositional age of the regional Gingin Chalk (Santonian, 86.3-83.6 Ma, ages from Cohen et al. 2013) has been previously cited as a minimum age constraint on the formation of the Yallalie structure, as clasts of Gingin Chalk have not been identified in the Mungedar breccia or from the two cores within the structure (Dentith et al. 1999). The presence of clasts of the Molecap Greensand Formation of the Upper Cretaceous Coolyena Group

(Coniacian, 89.8-86.3, ages from Cohen et al. 2013) in the breccia currently provides the best estimate for the maximum age constraint of the structure (Dentith et al. 1999).

Shock Deformation Features in Quartz

Quartz is widely used to document shock deformation, as it is abundant in crustal rocks and is rather resistant to alteration. Planar fractures (PFs) form at relatively low pressures (~5-10 GPa) and consist of open fractures with spacings from 10-15 µm that form in specific crystallographic orientations (e.g. Stöffler and Langenhorst 1994; French and Koeberl 2010; Poelchau and Kenkmann 2011). Quartz grains with multiple sets of planar fractures have been experimentally produced during shock recovery experiments, and form when pressures exceed the hugoniot elastic limit at ca. 5-10 GPa (Poelchau and Kenkmann, 2011). Shocked quartz grains containing well-developed planar fractures have been used to help confirm many impact events, including at the Rock Elm (French et al. 2004), Keurusselkä (Ferrière et al. 2010b), Hummeln (Alwmark et al. 2015), Saqqar (Kenkmann et al. 2015) and Decorah (French 2018) impact structures and elsewhere (see Poelchau and Kenkmann, 2011). We note that within the impact cratering community some workers question whethor or not multiple sets of PFs in quartz represent diagnostic evidence of shock-deformation, as quartz grains with PFs (i.e., generaly one single set, rarely more) have been reported from non-impact settings (see discussion in French and Koeberl, 2010). To avoid potential ambiguity in interpreting the significance of fractures in putative shocked quartz grains, in this study we adhere to a strict criteria for identification of shock-produced planar fractures in quartz. Our criteria required that: a) grains must contain one or more sets of evenly spaced, parallel planar factures that are pervasive across the grain, and b) the orientation of each set of planar fractures must correspond to crystallographic planes that have been demonstrated to form shock features previously.

Planar deformation features (PDFs) form at higher pressures (10-30 GPa) and consist of narrow, individual lamellae of amorphous SiO_2 in parallel (multiple) sets spaced 2-10 μm apart. Similar to PFs, the orientations of PDFs are crystallographically controlled. The high-pressure polymorphs coesite and stishovite, as well as diaplectic quartz glass and melted quartz (i.e., lechatelierite) may also form at elevated pressures and temperatures, depending on the properties of the target rocks, and local impact conditions (Stöffler and Langenhorst 1994). During reversion from high temperature conditions, silica can also form a distinctive texture called "ballen silica" which is commonly observed in impactites (Ferrière et al. 2009a, 2010a).

SAMPLES AND METHODS

For this study, samples of Mungedar Breccia were collected from two different outcrops located approximately 4 km west of the rim of the Yallalie structure (Fig. 2). The breccia samples were selected to search for microstructural evidence of shock deformation in minerals, in both rock and mineral clasts, as well as grains in the clastic matrix. The samples include both clast-poor and clast-rich polymictic breccia varieties. The breccia consists of green, tan and brown coloured rocks that contain a variety of different clasts in a quartz–rich, sand-dominated matrix. Crude layering is locally visible in outcrop (Fig. 3) and in thin section.

Samples were cut into slabs and impregnated with epoxy prior to preparing polished thin sections (Fig. 4). A search for shocked minerals was conducted using a petrographic microscope and scanning electron microscopy (SEM) at Curtin University on clast-rich breccia sample 16YA09 (nine thin sections) and clast-poor breccia sample 16YL01 (two thin sections) (Fig. 5). In addition to searching for shocked minerals, a systematic survey of clasts in the clast-rich breccia sample was conducted. Optical microscopy was used to survey the sections for shocked minerals, and energy dispersive spectroscopy with an SEM was used to determine the elemental composition of both lithic clasts and grains with possible shock features. Two grains of quartz (Q4 and Q6) were further mapped by electron backscatter diffraction (EBSD) using a Tescan Mira3 field emission SEM at Curtin University to evaluate the microstructure of grains with PDFs and PFs. The EBSD data were collected using the Oxford program Aztec, and maps were prepared with the Tango module in the Oxford software HKL Channel5. The EBSD patterns were indexed using a match unit for quartz from the HKL database (Sands 1969). Quartz grain Q4 was mapped with a 1.75 µm step size, and Q6 was mapped with a 0.5 µm step size. EBSD data are shown in texture component maps, where colors indicate either variations in lattice orientation or the presence of Dauphiné twins (Wenk et al. 2011).

Crystallographic orientations of PFs and PDFs in grains of shocked quartz were determined using a four-axis universal stage (u-stage) at the University of Vienna. A Horiba LabRAM HR Evolution Raman microscope, also at the University of Vienna, was used to identify silica polymorphs present in the samples. In addition to searching for shocked quartz, we also conducted a preliminary survey to search for detrital shocked zircon in Yallalie samples (e.g., Cavosie et al 2010), but have thus far not identified any shocked accessory phases.

The iSALE shock physics hydrocode (Amsden et al. 1980; Collins et al. 2004; Wünnemann et al. 2006) was used to model the formation of the Yallalie structure in order to determine the shock-level of material within proximal ejecta. The cell resolution in a 2D numerical mesh was 25 by 25 m. The projectile used in the simulation was 1.2 km in diameter, impacting Earth at 12 kms^{-1} vertical speed; this speed also represents faster speeds at moderately oblique impact angles (e.g., Pierazzo and Melosh 2000). The impactor was modelled using a dunite analytical equation of state (ANEOS) (Benz et al. 1989) representative of a stony asteroid. The most voluminous target rocks at Yallalie are the Jurassic Yarragadee Formation, and potentially the underlying Cattamarra Coal Measures (Higgins 1988; Economo 1991; Olierook et al. 2015; Timms et al. 2015). Quantitative analysis of both of these formations in nearby Gingin-1 and Gingin-2 wells illustrate that they are dominated by quartz arenite to arkose with minor heterolithic siltstone and shale, and variable proportions of water-filled porosity, typically up to ~30% at 500 m dropping systematically to <10% at ~3.5 km depth (Delle Piane et al. 2013; Timms et al. 2015). Therefore, the target was simulated using the ANEOS equation of state for granite (Pierazzo et al. 1997). Although granite is not present among the target rocks where the Yallalie structure formed, it may more accurately represent the target rock mineralogy than monomineralic quartzite. Granite is also a validated material for modelling crater formation in hydrocodes (Pierazzo et al. 1997). We acknowledge some level of uncertainty of the material properties of Perth Basin rocks at the time of the Yallalie impact.

RESULTS

Petrology of the Mungedar Breccia

The matrices of both clast-rich and clast-poor breccia samples are similar, and are mainly composed of angular to sub-rounded quartz grains with minor alkali feldspar and micas. Most matrix quartz grains range in size from 50 to150 µm, although larger grains are present. Lithic clasts within the clast-rich breccia are angular to sub-rounded, with at least four different lithologies present, including mudstone, glauconitic sandstone, siltstone, and palaeosol (Table 1). Mudstone is the most abundant lithology among lithic clasts surveyed, comprising 36 of 66 clasts. Mudstone clasts are brown, very fine-grained and range in size from 0.1 to 1.2 cm (Table 1). Some mudstone clasts contain deformed biotite grains (Fig. 6). A total of four biotite grains with kink-bands were identified in two different mudstone clasts. Glauconitic sandstone clasts (greensand) represent the second most abundant lithic clast type, comprising 18 of 66 clasts surveyed (Table 1). Greensand clasts range in size from 0.2 to 2 cm across, and have a distinctive green colour in hand sample (Figs. 3A, 4A). Greensand clasts consist of aggregates of rounded ~1 µm glauconite grains with minor amounts of detrital quartz and feldspar. The mudstone and greensand clasts are both texturally heterogeneous, and locally contain large quartz and feldspar grains that are easily distinguished from grains forming the matrix. Two other lithologies were encountered. One is represented by a single 3 mm-long quartz-rich siltstone clast (Fig. 5B), whereas the other is represented by a single 40 mm-long, elongate, dark orange to brown palaeosol clast (Table 1). Minor veins are also present.

Shocked Quartz Grains - optical imaging

A total of twenty-one grains with planar fractures (PFs) were identified. Eighteen sub-rounded to angular quartz grains with PFs were identified in the nine thin sections of the clast-rich breccia (sample 16YA09), and three in the clast-poor breccia (sample 16YL01). The PF bearing grains range in diameter from 150 µm to 1.2 mm. Fifteen occur as single grains in the matrix of the breccia, and the other six grains were found within mudstone clasts. The PFs are well-developed and cut across the entire grain in most cases, but are also localised within parts of the grains in others (e.g., Figs. 7,8). The PFs within each grain are typically spaced between 10 to 20 µm apart. PFs in all grains were indexed using the u-stage and found to be oriented along known crystallographic orientations for PFs in quartz (Table 2). Each grain contains two to five sets of PFs that are oriented along four main crystallographic planes (Table 2). Some PFs appear slightly curved (i.e., not perfectly planar) in crystal-plastically strained quartz grains. However, these PFs are locally planar and appear to be strictly crystallographically controlled; their deflections appear to follow crystallographic orientation variations in the host grain.

A total of six quartz grains with decorated PDFs were identified; all from the matrix of breccia sample 16YA09 (Fig. 9). The grains are sub-rounded to angular and are 100 µm to 4 mm in size, respectively. PDFs in all grains (9 sets) were also indexed using the u-stage and found to be oriented along known crystallographic orientations for PDFs in quartz (Table 2). One grain contains four orientations of PDFs, however only two are visible on the untilted surface under the optical microscope (Fig. 9F). During close inspection of the planar microstructures at high magnification, two additional PDF orientations were identified using the u-stage; the brownish appearance of the grain is the result of the dense network of PDFs.

Shocked Quartz Grains - orientation mapping

Orientation mapping using EBSD was conducted on part of a large quartz grain (Q4) that contains four orientations of planar fractures (Figs. 7A, 10A). The orientation map reveals two types of orientation domain; domains consisting of the host orientation, and domains with irregular boundaries in a Dauphiné twin orientation that are misoriented from the host grain by 60°/<0001> (Fig. 10B). The host and twin domains preserve up to 10° of distributed lattice misorientation across the area analyzed. The Dauphiné twin domains are pervasively distributed throughout the mapped area, and in many cases their boundaries terminate against the dominant set of $\{11\bar{2}2\}$ planar fractures.

A second orientation map was made on a quartz grain with decorated (0001) PDFs that were measured by u-stage (Fig. 10C). In contrast to the PF-bearing grain (Fig. 10B), the PDF-bearing grain contains relatively few Dauphiné twins (Fig. 10D). The orientation map reveals <10˚ of misorientation throughout the grain, much of which appears to be accommodated along low-angle boundaries (LABs), which are the dominant top-left to bottom-right oriented features visible in the map (Fig. 10D). Some of the LABs are planar, whereas others are irregular; the latter LABs locally form the boundaries of sub-grains (top left area of Fig. 10D). The dominant set of top-left to bottom-right planar LABs are conspicuously parallel to the measured (0001) PDF orientation (Fig. 10D), and thus may have formed in association with the PDFs during impact.

Ballen Silica

One elongate, ~1 mm-long silica grain in clast-poor breccia sample 16YL01 was found to exhibit a well-developed ballen texture (Fig. 11). The ballen texture is developed throughout the grain, but is most visible near the grain margin where the presence of secondary mineral films makes the texture more prominent. The ballen grain exhibits a uniform extinction in cross-polarized light (Fig. 11B). MicroRaman spectra collected from several points on the grain yield similar results that all show a dominant peak at 464 cm^{-1} that is associated with an O-Si-O bending mode (Ling et al. 2011), as well as other minor peaks at 127, 205, 264, 355, and 805 cm^{-1}. These peaks are all characteristic of unshocked α-quartz (McMillan et al. 1992), and no evidence of other silica polymorphs was detected. The uniform extinction of the ballen in cross-polarized light (Fig. 11B) and the fact that the grain is α-quartz further identifies the grain as type II ballen according to the classification scheme of Ferrière et al. (2009a, 2010a). Type II ballen grains have only been reported in rocks associated with meteorite impacts (Ferrière et al. 2009a).

iSALE Numerical Modelling of Yallalie Crater Formation

Impact simulation of the Yallalie crater formation produced a good match with sub-surface structural maps from published seismic surveys and borehole stratigraphy (Dentith et al. 1999; Hawke et al. 2006) (Fig. 12). The simulation shows a central uplift that is approximately 4 km in diameter and vertically displaces stratigraphy by up to 2 km. The final crater depth is ≤1 km. Fault traces previously interpreted from seismic data (Hawke et al. 2006) match well with fault traces suggested by the simulation, within a 5 km radius (Fig. 12). The iSALE simulation further suggests that the crater rim diameter may be larger than previously estimated, approximately 14 km (if measured at pre-impact surface level), or a 16 km diameter if measured rim-to-rim.

The spatial distribution and shock-level provenance of material forming the ejecta deposit are calculated from the iSALE simulation (Fig. 12). The Mungedar Breccia sample site (Fig. 2) corresponds to an approximate 10 km distance from the centre of the crater. In the iSALE model, the ejecta blanket geometry at the breccia sample site was taken to be 200 m wide and 100 m deep (as denoted by the grey box in Fig. 12). Each numerical cell was tracked by a mass-less tracer particle, which provides information about the material change with the flow. Analysis of each tracer particle inside the grey box shows that the ejecta at this site is composed of 75% mass that is shocked to peak pressures lower than 5 GPa, 17% of mass shocked to 5-10 GPa, and 8% mass shocked to peak pressures above 10 GPa. Due to computational limitations, some of the mass-less tracer particles are lost during the contact and compression cratering phase from numerical cells that experience the largest tension or extension. Therefore, the 8% of mass shocked at the highest pressures (reported here) may be higher in reality. Further analyses suggested that the proportions of shocked ejecta were moderately insensitive to variations in the size of the sampling area (grey box, Fig. 12); for example, a 100% increase in the width of the sampled area results in a <10% variation in the shock provenance statistics at this locality.

DISCUSSION

Evidence of Shock Deformation at Yallalie

Documentation of diagnostic shock features in quartz remains one of the most reliable methods available to confirm an impact event (e.g., French 1998; French and

Koeberl 2010; Alwmark et al. 2014, Kenkmann et al. 2015; Holm-Alwmark et al. 2018). Within the eleven thin-sections of Mungedar Breccia surveyed, a total of twenty-seven shocked quartz grains were identified, including twenty-one with up to 5 sets of PFs and six with up to 4 sets of PDFs. All of the planar microstructures in the grains were indexed by u-stage, and are in orientations that are diagnostic of shocked quartz. The orientations of indexed PFs (Table 2) record pressures from 5 to 10 GPa, while the orientations of indexed PDFs (Table 2) record pressures from 7.5 to 20 GPa. Of the twenty-seven shocked quartz grains identified, six PF-bearing grains occur in mudstone clasts (e.g., Fig. 7C,D), which definitively establishes mudstone as a shocked target rock. We interpret these findings to represent the first diagnostic evidence of hypervelocity processes documented within the Mungedar Breccia, which allows an impact origin for these components to be confirmed. Based on the presence of PFs and PDFs in matrix quartz, we estimate that these grains experienced pressures from 5-20 GPa, whereas quartz grains with PFs in the mudstone clasts experienced pressures of <10 GPa (Stöffler and Langenhorst 1994; Poelchau and Kenkmann 2011; Holm-Alwmark et al. 2018).

Shocked quartz grains in Mungedar Breccia are interpreted to have been excavated from the Yallalie structure during the impact event. However, we also consider the possibility that the provenance of shocked quartz and other grains identified in this study (ballen silica, deformed biotite) in Mungedar breccia did not form during the Yallalie impact event, and instead originated as detrital shocked grains (e.g., Cavosie et al. 2010) in siliciclastic rocks from the pre-impact stratigraphy at Yallalie. This scenario is considered unlikely, as no other impact structures are known regionally in the well-characterized stratigraphy of the Perth Basin. The close proximity (~4 km) of breccia outcrops in relation to the rim of the Yallalie structure, the presence of multiple grains of shocked quartz containing PFs and PDFs, a grain of ballen α-quartz, the presence of shocked lithic clasts with both PF-bearing quartz grains and deformed biotite grains, and the absence of comparable polymict breccias regionally, all support the interpretation that the Mungedar Breccia represents impact ejecta from the Yallalie structure. The closest known impact structures with ages older than the basement stratigraphy at Yallalie (i.e., pre-Jurassic) and that could have contributed detrital shocked grains are all located >500 km from Yallalie (Earth Impact Database 2018). Moreover, no large-scale regional fluvial or glaciogenic systems, the latter unlikely during the Cretaceous, are known that could have delivered detrital shocked grains from the older impact structures over the required distances, as has been demonstrated elsewhere (e.g., Erickson et al. 2013; Thomson et al., 2014; Montalvo et al. 2017). It is also highly unlikely that the cm-scale shocked mudstone clasts would survive multiple sedimentary cycles.

Deformation microstructures in the PF-bearing quartz grains described here from the Mungedar Breccia are similar to shocked quartz grains with PFs from the Rock Elm impact structure (USA), a 6.5-km-diametar structure formed in Cambrian sandstone (French et al. 2004). PFs in shocked quartz were the principal evidence used to confirm a hypervelocity origin for Rock Elm, as PDFs in quartz have not been reported from that site. We note that an absence or low abundance of quartz grains with PDFs does not preclude discovery of other higher-pressure shock indicators, given that reidite, a high-pressure $ZrSiO_4$ polymorph that forms at >30 GPa, was later reported in polymict sandstone breccia from the central uplift at Rock Elm (Cavosie et al. 2015). Shocked quartz grains with PFs have been reported at an increasing number of impact structures; a review by Poelchau and Kenkmann (2011) lists 26 impact structures where PFs (and feather features, another shock-related feature) have been reported in shocked quartz; PFs in quartz were most recently documented at the newly discovered ~5.5 km diameter Decorah structure in Iowa, USA (French et al. 2018).

Other Evidence of Impact Processes at Yallalie

Additional lines of evidence that are commonly associated with, but not diagnostic of, impact processes were found in this study. These include a quartz grain with type-II ballen texture, kink-bands in biotite, and Dauphiné twins in shocked quartz grains.

Ballen silica is indicative of impact, although it is not considered as diagnostic evidence of shock metamorphism. Ballen silica (shown here to be Type II, α-quartz) forms upon cooling from ß-quartz formed either by a solid-solid transformation involving diaplectic quartz glass, or a solid-liquid transformation involving lechatelierite (Ferrière et al. 2009a); either could have originated in melt formed during the Yallalie impact event, although no occurrences of impact melt have been reported that could better establish its provenance.

Biotite grains with kink-bands (Fig. 6) provide evidence for the deformation of biotite, and so-called shocked mica grains have long been recognized in bedrock from established impact structures (e.g., Schneider 1972). However, kink-bands in biotite alone do not provide diagnostic evidence of shock deformation, as they also form during endogenic deformation (e.g., Misra and Burg 2012). We note that in our survey of 36 mudstone clasts (Table 1), deformed biotite grains were only found in two clasts, both of which also contain shocked quartz grains with PFs. These two clasts, tentatively identified as Jurassic Yarragadee Formation, currently represent the only documented shocked target rock fragments from the Yallalie structure (Fig. 7C).

Orientation maps show that both PF- and PDF-bearing shocked quartz grains from Yallalie contain Dauphiné twins (Fig. 10). Dauphiné twins in quartz can form under low stresses and stress rates that are associated with a wide range of endogenic processes (e.g., Hartley and Wilshaw 1973; Rahl et al. 2018). Therefore, Dauphiné twins do not provide diagnostic evidence of shock deformation per se, but they have been reported in PDF-bearing shocked quartz grains from the Vredefort Dome (Wenk et al. 2011), Charlevoix (Trepmann and Spray 2007), and Rochechouart (Hamers et al. 2017) impact structures. Termination of Dauphiné twin boundaries against PFs in the quartz grains in this study suggests that they formed late during the impact deformation sequence, with their propagation impeded against pre-existing PFs.

The Mungedar Breccia: primary or secondary ejecta?

The Mungedar Breccia is here shown to be a product of impact due to the presence of shocked quartz grains, as well as lithic clasts (mudstone) that contain shocked quartz. However, the question of whether the breccia represents a primary ejecta deposit, or one that has been subsequently re-worked, remains unresolved; below we discuss various lines of evidence to further explore the nature of the breccia.

The crude layering observed in breccia outcrops (Fig. 3) may have resulted from primary deposition of the ejecta into a shallow water column. However, we cannot exclude the possibility that the layering may also have resulted from subsequent reworking. Shock levels experienced by clasts in the breccia, as recorded by deformation microstructures in quartz (i.e., 5-20 GPa), are consistent with results of model simulations of shock level in the primary ejecta blanket at the locations where breccia was sampled, which is in turn consistent with a primary origin for the ejecta. However, if localized reworking of the breccia occurred after deposition, the distribution of shocked material may not have changed significantly. Likewise, the overall low abundance of material shocked above 10 GPa in the modelled ejecta blanket (<10%) appears to agree with the overall low abundance of shocked quartz grains identified (twenty-seven grains in 11 thin sections). However, local reworking could also have diluted an originally higher abundance of shocked minerals in the analyzed material.

The presence of a grain of ballen silica (Fig. 11) as a mineral clast in a sandstone breccia that clearly did not melt (Fig. 5A) could be interpreted as evidence for reworking of the original host rock (or melt) in which the ballen silica formed. However, flow paths during crater excavation characteristically produce mixtures of both unshocked and highly shocked material in ejecta (Melosh 1989), and so there is no conclusive evidence that the clast-poor breccia sample with ballen silica was reworked.

We tentatively interpret the Mungedar Breccia to be a primary ejecta deposit based on the overall good agreement between our petrographic observations and modelling results. However, as noted above, the data do not allow a secondary origin by reworking to be excluded. Regardless of the nature of the breccia (primary vs. secondary), given that the Yallalie structure is buried below 100-300 m of post-impact sedimentary rocks (Hawke et al. 2006), the exposures of the Mungedar Breccia at the present day surface indicate that it may have been deposited on relatively high paleotopography (Dentith et al. 1999).

Comparison of Mungedar Breccia with Other Impact Breccia

Breccia comprised primarily of lithic clasts in a quartz-sand matrix has been reported from other comparable-sized impact structures formed in sedimentary target rock. Some of these breccias have similarities with the Mungedar Breccia. Of these, the most similar may be that found at the Wetumpka impact structure in Alabama, USA, a 5-km-diameter structure formed at ~84 Ma in a shallow marine environment (King et al. 2015). At the Wetumpka structure, there are deposits of 'polymict impact breccia' that outcrop near the center of the structure (King et al. 2015). The Wetumpka surface polymict impact breccia is described as a heterogeneous lithic clast-bearing breccia, including local layering/laminations, with the dominant planar microstructures in shocked quartz in that unit being PFs and feature features, rather than PDFs (King et al. 2015). While many aspects of the Wetumpka surface polymict impact breccia appear similar to the Mungedar Breccia, the emplacement mechanisms cited at Wetumpka include gravity-driven slumping and resurge (King et al. 2015). The location of the Mungedar Breccia beyond the rim of the Yallalie impact structure effectively rules out resurge, however, it is possible that slumping may have played a role if the Mungedar Breccia was originally deposited on paleotopographic high surfaces or slopes.

An Upper Cretaceous Impact Structure in Western Australia

The discovery and characterization of PFs and PDFs in quartz grains from allochthonous breccia at the Yallalie structure allows the recognition of Yallalie as an established complex impact structure in Western Australia. The age of the Yallalie impact is currently only constrained by stratigraphic relations to be Upper Cretaceous (probably Santonian), as no materials appropriate for the use of radiometric dating techniques have been discovered thus far. The buried structure appears to be wellpreserved overall, as interpreted from geophysical surveys and the overlying post-impact sedimentary rocks (Hawke et al. 2006). This observation has been cited to argue that the Yallalie structure may have formed in a quiescent shallow marine environment and was buried quickly (Dentith et al. 1999; Hawke et al. 2006). Such an environment would be similar to, for example, the Lockne (Sturkell 1998), Rock Elm (French et al. 2004), and Flynn Creek (Schieber and Over 2005) impact structures. Studies have shown that shallow marine impacts can result in rapid crater burial shortly after the impact, limiting erosion and thus enhancing crater preservation (Dypvik et al. 2004). However, conclusive evidence for a terrestrial vs. marine setting for the Yallalie impact remains elusive, and requires further study.

CONCLUSION

Our survey revealed evidence of shock metamorphism within the Mungedar Breccia at the Yallalie structure, resulting in the recognition of Yallalie as a newly established impact structure in Western Australia. The PFs and PDFs found in twenty-seven quartz grains that were characterized using u-stage provide diagnostic evidence of shock deformation, and confirm that these quartz grains and the lithic clasts that contain them experienced shock pressures from 5-20 GPa. Previous geophysical studies reported structural disturbances created by the 12 km diameter Yallalie structure (Hawke 2004). Complementary to existing observations, our iSALE modelling of ejecta geometry and shock characteristics suggests the Yallalie impact structure may be up to 14-16 km in rim diameter. The Earth Impact Database currently lists 27 impact structures within Australia (*Earth Impact Database*, 2018); confirmation of a hyper-velocity impact origin for the Yallalie structure increases the number of confirmed impact structures in Australia to 28.

ACKNOWLEDGEMENTS

Support was provided by the NASA Astrobiology Program (grant NNAI3AA94A) and a Curtin Research Fellowship to AJC. Support was also provided by the Space Science and Technology Centre and the Microscopy and Microanalysis Facility in the John de Laeter Centre and Curtin University. We thank M. Aspandiar for discussions about paleosol petrography. L. Young assisted with field work, and local land owners are thanked for access to private property. C. Koeberl provided access to the universal-stage at the University of Vienna, and L. Nasdala and C. Chanmuang provided access and assistance to the Raman microscope at the University of Vienna. We also acknowledge the developers of the iSALE hydrocode. We thank C. Awlmark and an anonymous reviewer for helpful and constructive review comments, and W.U. Reimold for providing critical comments and also editorial handling.

REFERENCES

Alwmark C., Alwmark-Holm S., Ormö J., and Sturkell E. 2014. Shocked Quartz Grains from the Målingen Structure, Sweden-Evidence for a Twin Crater of the Lockne Impact Structure. *Meteoritics & Planetary Science* 49(6):1076–1082.

Alwmark C., Ferrière L., Holm-Alwmark S., Ormö J., Leroux H., and Sturkell E. 2015. Impact Origin for the Hummeln Structure (Sweden) and Its Link to the Ordovician Disruption of the L Chondrite Parent Body. *Geology* 43(4):279–282.

Amsden A. A., Ruppel H. M., and Hirt C. W. 1980. SALE: A Simplified ALE Computer Program for Fluid Flow at all Speeds. Report LA-8095. Los Alamos National Laboratories, N. Mex. 105 pp.

Benz W., Cameron A. G. W., and Melosh H. J. 1989. The Origin of the Moon and the single-impact hypothesis III. *Icarus* 81:113-131.

Bevan A. 2012. Yallalie Impact Structure, In: Western Australian Impact Craters, Field Excursion. Excursion Guidebook for the 75th Annual Meeting of the Meteoritical Society, Cairns, Australia.

Bevan A., Hough R., and Hawke P. 2004. Morphology and Origin of an Allocthonous Breccia Near the Yallalie Structure, Western Australia: Evidence for Subaqueous Impact? *AGC abstract* 227.

Carter J. D., Lipple S. L and Geological Survey of Western Australia. 1982. Moora, Western Australia: sheet SH/50-10 international index. Geological Survey of Western Australia, Perth, W.A

Cavosie A. J., Erickson T. M., and Timms N. E. 2015. Nanoscale Records of Ancient Shock Deformation: Reidite ($ZrSiO_4$) in Sandstone at the Ordovician Rock Elm Impact Crater. *Geology* 43(4):315–318.

Cavosie A. J., Quintero R. R., Radovan H. A. and Moser D. E. 2010. A Record of Ancient Cataclysm in Modern Sand: Shock Microstructures in Detrital Minerals from the Vaal River, Vredefort Dome, South Africa. *Geological Society of America Bulletin* 122:1968–1980.

Cockbain A. E. 1990. Perth basin. Geology and Mineral Resources of Western Australia. Western Australia Geological Survey, Memoir, 3:495–524.

Cohen K. M., Finney S. C., Gibbard P. L., and Fan J.-X. 2013. The ICS International Chronostratigraphic Chart. *Episodes* 36(3):199-204.

Collins G. S., Melosh H. J., and Ivanov B. A. 2004. Damage and Deformation in Numerical Impact Simulations. *Meteoritics & Planetary Science* 39:217–231.

Delle Piane C., Esteban L., Timms N. E., and Ramesh Israni, S. 2013. Physical Properties of Mesozoic Sedimentary Rocks from the Perth Basin, Western Australia. *Australian Journal of Earth Sciences* 60(6–7):735–745.

Dentith M. C., Bevan A. W. R., and Mcinerney K. B. 1992. A Preliminary Investigation of the Yallalie Basin: a Buried 15 km Diameter Structure of Possible Impact Origin in the Perth Basin, Western Australia. *Meteoritical society Meeting Abstract*.

Dentith M. C., Bevan A. W. R., Backhouse J., Featherstone W. E., and Koeberl C. 1999. Yallalie: A Buried Structure of Possible Impact Origin in the Perth Basin, Western Australia. *Geological Magazine* 136(6):619–632.

Dypvik H., Burchell M. J., and Claeys P. 2004. Impacts into Marine and Icy Environments — A Short Review. In Cratering in Marine Environments and on Ice, 1–20. Impact Studies. Heidelberg: Springer Berlin.

Earth Impact Database. 2018. http://www.unb.ca/passc/ImpactDatabase/. Accessed September 7, 2018.

Erickson T. M., Cavosie A. J., Moser D. E., Barker I. R., Radovan H. A., and Wooden J., 2013. Identification and provenance determination of distally transported, Vredefort-derived shocked minerals in the Vaal River, South Africa using SEM and SHRIMP-RG techniques. *Geochimica et Cosmochimica Acta*, 107:170–188.

Economo M. 1991. Perth Basin EP 321, Western Australia, Yallalie No. 1 Well Completion Report. Ampol Exploration Ltd. (unpublished).

Engelhardt W. v. and Bertsch W. 1969. Shock-induced Planar Deformation Structures in Quartz from the Ries Crater, Germany. *Contributions to Mineralogy and Petrology* 20:203–234.

Ferrière L. and Osinski R. 2013. Shock Metamorphism. In *Impact Cratering: Processes and Products*, edited by Osinski G. R. and Pierrazo E. Oxford: Wiley-Blackwell. pp. 106–124.

Ferrière L., Koeberl C., and Reimold W. U. 2009a. Characterisation of Ballen Quartz and Cristobalite in Impact Breccias: New Observations and Constraints on Ballen formation. *European Journal of Mineralogy* 21(1):203–217.

Ferrière L., Morrow J. R., Amgaa T., and Koeberl C. 2009b. Systematic Study of Universal-Stage Measurements of Planar Deformation Features in Shocked Quartz: Implications for Statistical Significance and Representation of Results. *Meteoritics and Planetary Science* 44(6):925–940.

Ferrière L., Koeberl C., Libowitzky E., Reimold W. U., Greshake A., and Brandstätter F. 2010a. Ballen Quartz and Cristobalite in Impactites: New Investigations. *Geological Society of America Special Paper* 465:609–618.

Ferrière L., Raiskila S., Osinski G. R., Pesonen L. J., and Lehtinen M. 2010b. The Keurusselkä Impact Structure, Finland—Impact Origin Confirmed by Characterization of Planar Deformation Features in Quartz Grains. *Meteoritics & Planetary Science* 45(3):434–446.

French B. M. 1998. Traces of Catastrophe: A Handbook of Shock-Metamorphic Effects in Terrestrial Meteorite Impact Structures. Houston: Lunar and Planetary Science Institute.

French B. M., Cordua W. S., and Plescia J. B. 2004. The Rock Elm Meteorite Impact Structure, Wisconsin: Geology and Shock-Metamorphic Effects in Quartz. *Geological Society of America Bulletin* 116(1–2):200–218.

French B. M., and Koeberl C. 2010. The Convincing Identification of Terrestrial Meteorite Impact Structures: What Works, What Doesn't, and Why. *Earth-Science Reviews* 98(1–2):123–170.

French B. M., McKay R. M., Liu H. P., Briggs D. E.G., Witzke B. J. 2018. The Decorah Structure, Northeastern Iowa: Geology and Evidence for Formation by Meteorite Impact. *Geological Society of America Bulletin* doi:https://doi.org/10.1130/B31925.1

Hamers M. F., Pennock G. M., and Drury M. E. 2017. Scanning Electron Microscope Cathodoluminescence Imaging of Subgrain Boundaries, Twins and Planar Deformation Features in Quartz. *Physics and Chemistry of Minerals* 44:263–275.

Harris L. B. 1994. Structural and Tectonic Synthesis for the Perth Basin, Western Australia. *Journal of Petroleum Geology* 17(2):129–156.

Hartley N. E. W., and Wilshaw T. R. 1973. Deformation and Fracture of Synthetic α-quartz. *Journal of Materials Science* 8(2):265-278.

Hawke P. J. 2004. The Geophysical Signatures and Exploration Potential of Australia's Meteorite Impact Structures. Ph.D. thesis, University of Western Australia, Perth, Western Australia, Australia.

Hawke P. J., Buckingham A. J., and Dentith M. C. 2006. Modelling source depth and possible origin of magnetic anomalies associated with the Yallalie impact structure, Perth Basin, Western Australia. *Exploration Geophysics* 37:191–196.

Higgins R. 1988. Cypress Hill 1 - Well completion report for Ampol Exploration Ltd (unpublished).

Holm-Alwmark S., Ferrière L., Alwmark C. and Poelchau M. H. 2018. Estimating Average Shock Pressures Recorded by Impactite Samples Based on Universal Stage Investigations of Planar Deformation Features in Quartz—Sources of Error and Recommendations. *Meteoritics & Planetary Science* 53:110–130.

Huffman A. R., and Reimold W. U. 1996. Experimental Constraints on Shock-Induced Microstructures in Naturally Deformed Silicates. *Tectonophysics* 256(1):165–217.

Kenkmann T., Afifi A. M., Stewart S. A., Poelchau M. H., Cook D. J., and Neville A. S. 2015. Saqqar: A 34 km Diameter Impact Structure in Saudi Arabia. *Meteoritics & Planetary Science* 50(11):1925–1940.

King D. T., Morrow J. R., Petruny L. W., and Ormö J. 2015. Surficial Polymict Impact Breccia Unit, Wetumpka Impact Structure, Alabama: Shock Levels and Emplacement Mechanism. *Geological Society of America Special Paper* 518:149–164.

McMillan P. F., Wolf G. H., and Lambert P. 1992. A Raman Spectroscopic Study of Shocked Single Crystalline Quartz. *Physics and chemistry of minerals* 19(2):71–79.

Melosh H. J. 1989. Impact Cratering: A Geologic Process. New York: Oxford University Press.

Misra S., and Burg J. P., 2012. Mechanics of Kink-Bands During Torsion Deformation of Muscovite Aggregate. *Tectonophysics* 548: 22–33.

Montalvo S. D., Cavosie A. J., Erickson T. M., and Talavera C., 2017. Fluvial Transport of Impact Evidence from Cratonic Interior to Passive Margin: Vredefort-derived Shocked Zircon on the Atlantic Coast of South Africa. *American Mineralogist* 102(4):813–823.

Mory A. J., and Iasky R. P. 1996. Stratigraphy and Structure of the Onshore Northern Perth Basin, Western Australia. Geological Survey of Western Australia. Report 46.

Olierook H. K. H., Timms N. E., Wellmann J. F., Corbel S., and Wilkes P. G. 2015. 3D Structural and Stratigraphic Model of the Perth Basin, Western Australia: Implications for Sub-Basin Evolution. *Australian Journal of Earth Sciences* 62(4):447–467.

Pierazzo E., Vickery A. M., and Melosh H. J. 1997. A reevaluation of impact melt production. *Icarus* 127:408–423.

Pierazzo E. and Melosh H. J. 2000. Understanding Oblique Impacts from Experiments, Observations, and Modelling. *Annual Reviews in Earth and Planetary Science* 28:141–167.

Playford P. E., Low G. H., and Cockbain A. E. 1976. Geology of the Perth Basin, Western Australia. Geological Survey of Western Australia, 124 pp.

Poelchau, M. H., and Kenkmann T. 2011. Feather Features: A Low-Shock-Pressure Indicator in Quartz. *Journal of Geophysical Research* 116(B2).

Rahl J. M., McGrew A. J., Fox J. A., Latham J. R., & Gabrielson T. 2018. Rhomb-dominated crystallographic preferred orientations in incipiently deformed quartz sandstones: A potential paleostress indicator for quartz-rich rocks. *Geology* 46(3):195–198.

Sands D. E. 1969. Introduction to Crystallography. New York: WA Benjamin.

Schieber J., and Over D. J. 2005. Chapter 4 Sedimentary Fill of the Late Devonian Flynn Creek Crater: A Hard Target Marine Impact. Understanding Late Devonian And Permian-Triassic Biotic and Climatic Events. 51–69.

Schneider H. 1972. Shock-Induced Mechanical Deformations in Biotites from Crystalline Rocks of the Ries Crater (Southern Germany). Contributions to Mineralogy and Petrology 37:75–85.

Sircombe K. N., and Freeman M. J. 1999. Provenance of Detrital Zircons on the Western Australia coastline—Implications for the Geologic History of the Perth Basin and Denudation of the Yilgarn Craton. *Geology* 27(10):879–882.

Song T., and Cawood P. A. 2000. Structural Styles in the Perth Basin Associated with the Mesozoic Break-up of Greater India and Australia. *Tectonophysics* 317:55**e**72.

Stöffler D., and Langenhorst F. 1994. Shock Metamorphism of Quartz in Nature and Experiment: I. Basic Observation and Theory. *Meteoritics & Planetary Science* 29(2):155–181.

Sturkell E. 1998. The Marine Lockne Impact Structure, Jämtland, Sweden: A Review. Geologische Rundschau 87(3):253–267.

Thomson, O.A., Cavosie, A.J., Moser, D.E., Barker, I., Radovan, H.A., and French, B.M., 2014, Preservation of detrital shocked minerals derived from the 1.85 Ga Sudbury impact structure in modern alluvium and Holocene glacial deposits:

Geological Society of America Bulletin, v. 126, p. 720–737, https://doi.org/10.1130/B30958.1.

Timms N. E., Olierook H. K. H., Wilson M. E. J., Delle Piane C., Hamilton P. J., Cope P., and Stütenbecker L. 2015. Sedimentary Facies Analysis, Mineralogy and Diagenesis of the Mesozoic Aquifers of the Central Perth Basin, Western Australia. *Marine and Petroleum Geology* 60: 54–78.

Trepmann C. A., and Spray J. G. 2007. Shock-Induced Crystal-Plastic Deformation and Post-Shock Annealing of Quartz. *European Journal of Mineralogy* 18(2):161.

Veevers J. J., Saeed A., Belousova E. A., and Griffin W. L. 2005. U–Pb Ages and Source Composition by Hf-Isotope and Trace-Element Analysis of Detrital Zircons in Permian Sandstone and Modern Sand from Southwestern Australia and a Review of the Paleogeographical and Denudational History of the Yilgarn Craton. *Earth-Science Reviews* 68(3):245–279.

Wenk H., Janssen C., Kenkmann T., Dresen G. 2011. Mechanical Twinning in Quartz: Shock Experiments, Impact, Pseudotachylites and Fault Breccias. *Tectonophysics* 510:69–79.

Wünnemann K., Collins G. S., and Melosh H. J. 2006. A Strain-Based Porosity Model for Use in Hydrocode Simulations of Impacts and Implications for Transient Crater Growth in Porous Targets. *Icarus* 180:514–527.

TABLE

Table 1. Characteristics of objects in clast-rich breccia sample 16YA09.

clast type	length (mm)	colour (PPL)	grain size	grain shape	minerals
Lithic clasts					
mudstone n=36	1-12	brn	silt + clay + sand	sr to a	Qz, Afs, Bt, clay, Ilm
glauconitic sandstone n=18	2-20	grn/brn	sand + silt + clay	sr to sa	Qz, Afs, Zrn, Glt
siltstone n=1	3.5	grey	silt	sr to sa	Qz, Zrn, TiO2,
palaeosol n=1	40	drk or		r to sa	Qz, Glt
Other objects					
vein n=5	0.5-4 width	brn	clay	ind	clay, Qz, Afs, Ilm
opaque objects (Fe-rich clasts) n=5	1-3	opaque	sand/silt/clay	ind.	Qz, Glt

Notes: ind- indeterminate; grain shape: r = rounded; sr = sub-rounded, a = angular; sa = sub-angular; PPL= plane polarized light; Colours: lt.=light, brn=brown, drk=dark, grn=green, blk=black, or=orange; Minerals: Qz=quartz, Afs=alkali feldspar, Glt=glauconite, Bt=biotite, Ilm=ilmenite, Zrn=zircon

Table 2. Summary of PF and PDF set abundances and indexed PF and PDF crystallographic orientations in quartz grains from six thin sections from the Yallalie structure, as determined using the universal-stage.

	PF	PDF
No. of investigated grains	21	6
No. of measured sets	65	9
No. of sets/grain (N)	3.1	1.5
No. of sets/grain (N*)[a]	2.9	1.5

No. of sets; % relative to total no. of quartz grains examined; number of grains

	PF		PDF	
1 set	4.8	1	83	5
2 sets	28.6	6	n.d.	n.d.
3 sets	28.6	6	n.d.	n.d.
4 sets	28.6	6	16.7	1
5 sets	9.5	2	n.d.	n.d.
Total	100	21	100	6

Indexed PF and PDF crystallographic orientations; absolute frequency (%)[b]; number of sets

	PF		PDF	
c (0001)	13.8	9	11.1	1
a {1014}	n.d.	n.d.	n.d.	n.d.
ω {1013}	1.5	1	11.1	1
π {1012}	3.1	2	22.2	2
r, z {1011}	44.6	29	44.4	4
m {1010}	n.d.	n.d.	n.d.	n.d.
ξ {1122}	12.3	8	11.1	1
s {1121}	3.1	2	n.d.	n.d.
ρ {2131}	1.5	1	n.d.	n.d.
x {5161}	1.5	1	n.d.	n.d.
a {1120}	n.d.	n.d.	n.d.	n.d.
{2241}	3.1	2	n.d.	n.d.
{3141}	4.6	3	n.d.	n.d.
t {4041}	1.5	1	n.d.	n.d.
k {5160}	1.5	1	n.d.	n.d.
Unindexed	7.7	5	0.0	n.d.
Total	100	65	100	9

[a]Calculated only on indexed sets (i.e., unindexed sets excluded).
[b]Method described in, e.g., Engelhardt and Bertsch (1969) and Stöffler and Langenhorst (1994).
n.d. = none detected.

FIGURES

Figure 1. Location map of the Yallalie Structure in Australia. (A) Map of the Perth Basin, onshore sub-basins in the central-northern Perth Basin, and Yilgarn Craton (after Cockbain 1990; Mory and Iasky 1994). Filled squares indicate cities and towns. (B) Map of inset shown in A. The Yallalie structure is situated within the Dandaragan Trough, ~10 km west of the Darling Fault.

Figure 2. Location map and generalized geology of the area around the Yallalie structure (after Carter et al. 1982 and Dentith et al. 1999). The breccia study area is located in the lower left. The thick dashed line indicates the 12 km diameter size estimate previously suggested by Dentith et al. (1999).

Figure 3. Photographs of Mungedar Breccia outcrops. (A) A large, elongate clast of greensand (Molecap Greensand Fm.?) within the breccia. (B) Horizontal layering within the breccia. (C) Centimetre-sized clasts found within the breccia. The shaft of the chisel in all images is 2 cm wide.

Figure 4. Slabs of Mungedar Breccia from which thin-sections were made for this study. (A) Green-to-tan colored clast-rich breccia, sample 16YA09. (B) Example of brown-to-orange colored clast-poor breccia.

Figure 5. Thin-section scans of Mungedar Breccia samples. (A) Clast-poor sample 16YL01. The section was cut from a hand sample similar to that shown in Figure 4B, and was collected proximal to the outcrops in Figure 3. This section contains a grain of ballen quartz and three grains with PFs (see insets). (B) Clast-rich sample 16YA09. This section contains six shocked quartz grains; two with planar fractures and four with decorated planar deformation features (see insets). The section was cut from the hand sample shown in Figure 4A, and was collected proximal to the outcrops shown in Figure 3.

Figure 6. Backscattered electron images of deformed biotite grains with kink-bands in mudstone clasts from clast-rich Mungedar Breccia sample 16YA09. (A) Full grain image of a biotite grain with one orientation of kink bands in a sub-vertical orientation (see arrow in inset). (B) Full grain image of biotite grain with two orientations of kink-bands. (C) Detailed view of two orientations of kink-bands from (B). The arrows indicate orientations of the kink-bands. Note the small grain size.

Figure 7. Transmitted light images of shocked quartz grains with planar fractures from clast-rich Mungedar Breccia sample 16YA09. (A) Image of a siltstone clast (outlined with dashed line) containing shocked quartz grain Q7 and deformed biotite grains. (B) Detailed view of inset shown in A, showing a full grain image of grain Q7 with three orientations of indexed planar fractures. (C) Full grain image of shocked quartz grain Q1. (D) Detailed view of inset from C, showing two orientations of indexed planar fractures.

Figure 8. Transmitted light images of shocked quartz grains with planar fractures from clast-rich Mungedar Breccia sample 16YA09. (A) Full grain image of shocked quartz grain Q4. (B) Detailed view of inset shown in A, showing four indexed orientations of planar fractures. (C) Full grain image of shocked quartz grain Q3. (D) Detailed view of inset from C, showing four indexed orientations of planar fractures.

Figure 9. Transmitted light images of shocked quartz grains with decorated planar deformation features (PDFs) from clast-rich Mungedar Breccia sample 16YA09. (A) Full grain image of shocked quartz grain Q6, with the indexed PDF orientation. (B) Full grain image of shocked quartz grain Q2, with the indexed PDF orientation.(C) Full grain image of shocked quartz grain Q16 which contains 3 PF sets and PDF set. (D) Detailed view of inset shown in C, with the indexed PDF orientation. (E) Detailed view of inset shown in C, with the one orientation of indexed PDFs (labelled) and three orientations of indexed PFs. (F) Full grain image of shocked quartz grain Q24. Two orientations of PDFs are indicated on the figure; two additional sets are visible with the u-stage along {1011} and {1122} orientations. A close inspection of the planar microstructures under the u-stage at high magnification shows that the brownish appearance of the grain results from the dense network of microstructures.

Figure 10. Orientation maps of shocked quartz grains. (A) Plain polarized light image of a part of PF-bearing grain Q4 (see Figure 7A) that was mapped by EBSD. (B) Orientation map showing strain in the host grain using a texture component with a maximum misorientation of 10˚ (rainbow color scale). Dauphiné twins are shown in pink. (C) Plain

polarized light image of PDF-bearing grain Q6 that was mapped by EBSD. (D) Orientation map showing strain in the host grain using a texture component with a maximum misorientation of 10˚ (rainbow color scale). Dauphiné twins are shown in pink. LAB= Low angle boundary. Red cross in B and D indicates the reference orientation.

Figure 11. Type-II ballen quartz grain from clast-poor breccia sample 16YL01. (A) Plain polarized light image of the grain. (B) MicroRaman spectra confirming that the grain is α-quartz. The inset shows a cross-polarized light image exhibiting homogeneous extinction.

Figure 12. Numerical simulation of the Yallalie impact crater. Peak pressure is shown on the left and partial displacement is shown on the right (r = radius, z = height relative to the paleo surface). The grey box at the surface denotes the sampled ejecta site. This simulation was made in iSALE-2D hydrocode using a 1.2 km impactor striking a granite target at 12 km/s, forming a crater with a rim-to-rim diameter of 14-16 km. The grey image below the model is a previously published interpreted seismic line across the Yallalie structure (Bevan 2012). Interpreted fault traces on the seismic line (from Hawke et al. 2006) were added to the iSALE model at the same location and scale. TWT= two way time.

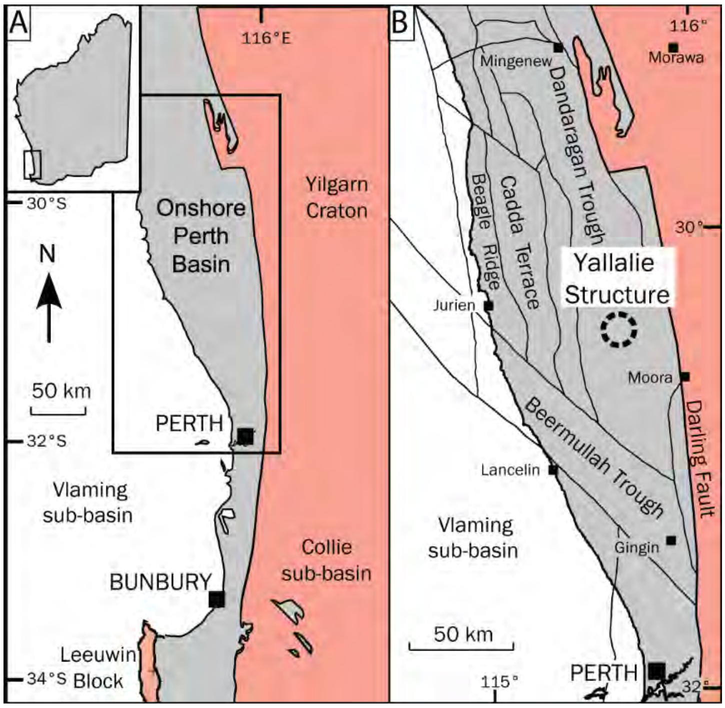
A
116°E
Yilgarn
Craton
30°S
Onshore
Perth
Basin
N
50 km
PERTH
32°S
Vlaming
sub-basin
Collie
sub-basin
BUNBURY
Leeuwin
34°S Block
B
116°
Mingenew
Morawa
Dandaragan Trough
Beagle Ridge
Cadda Terrace
30°
Yallalie
Structure
Jurien
Moora
Beermullah Trough
Darling Fault
Lancelin
Vlaming
sub-basin
Gingin
50 km
115°
PERTH
32°

Figure 1

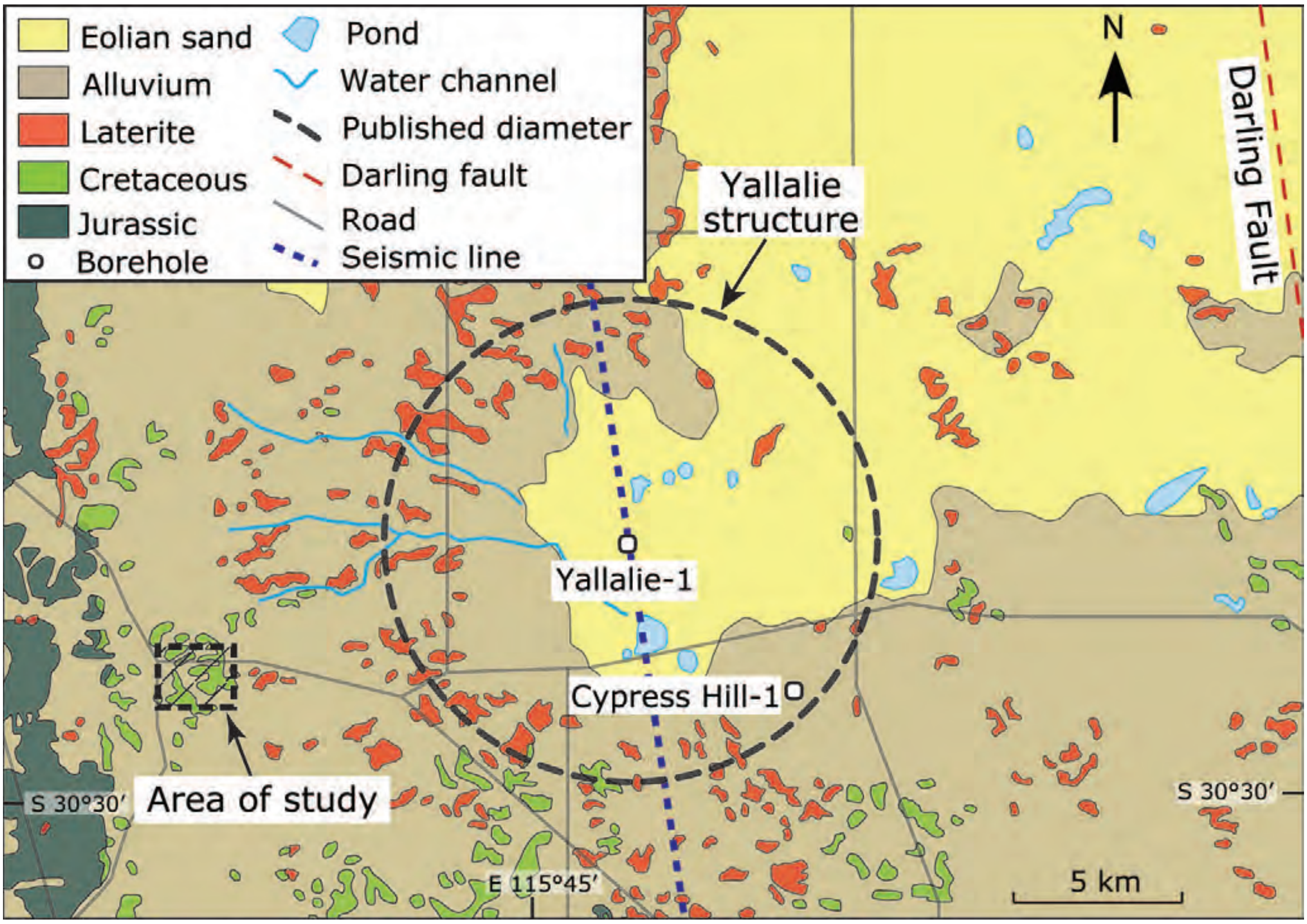
Eolian sand
Alluvium
Laterite
Cretaceous
Jurassic
Borehole
Pond
Water channel
Published diameter
Darling fault
Road
Seismic line
N
Darling Fault
Yallalie structure
Yallalie-1
Cypress Hill-1
Area of study
S 30°30′
S 30°30′
E 115°45′
5 km

Figure 2

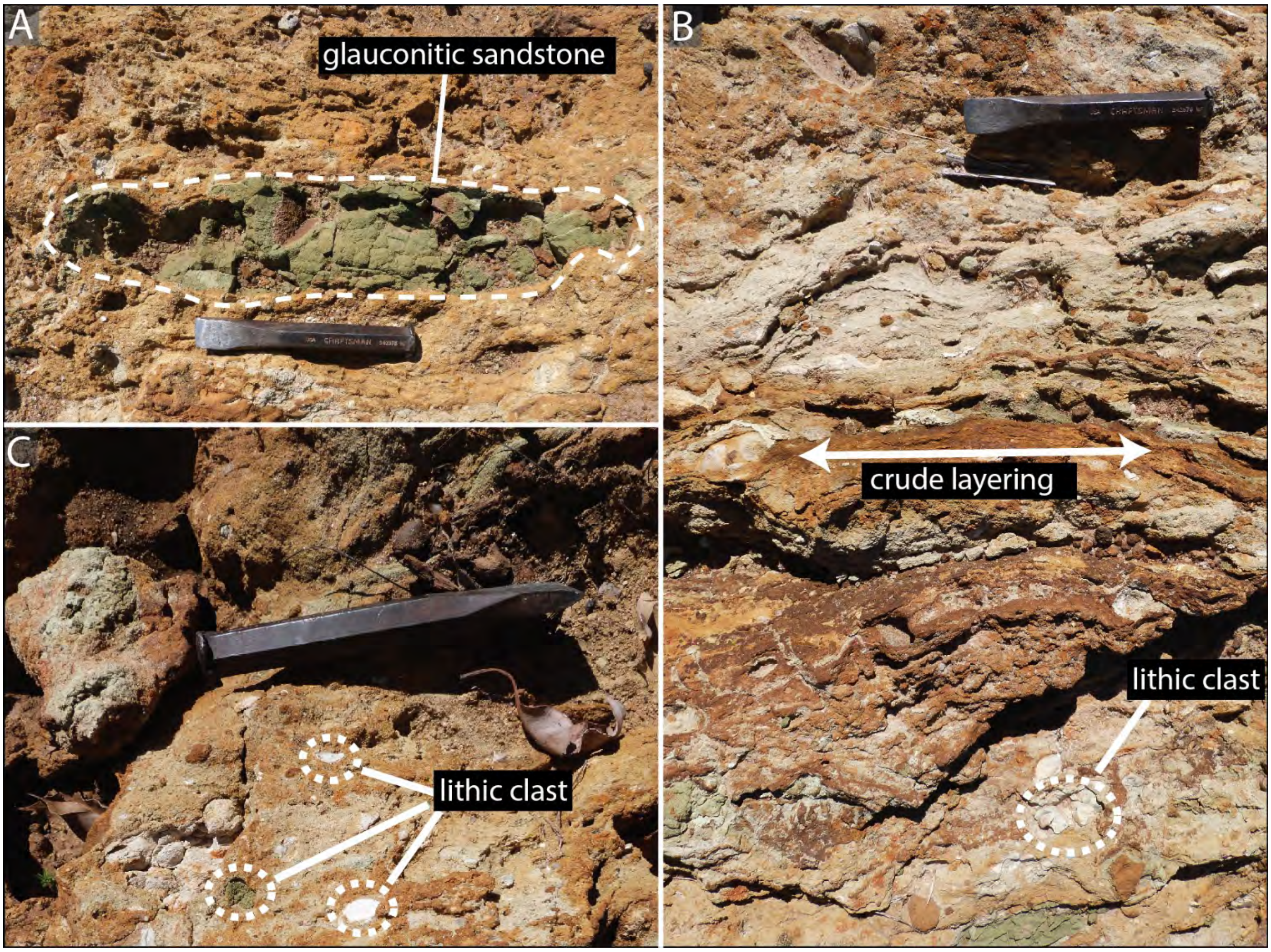
A
glauconitic sandstone
B
crude layering
lithic clast
C
lithic clast

Figure 3

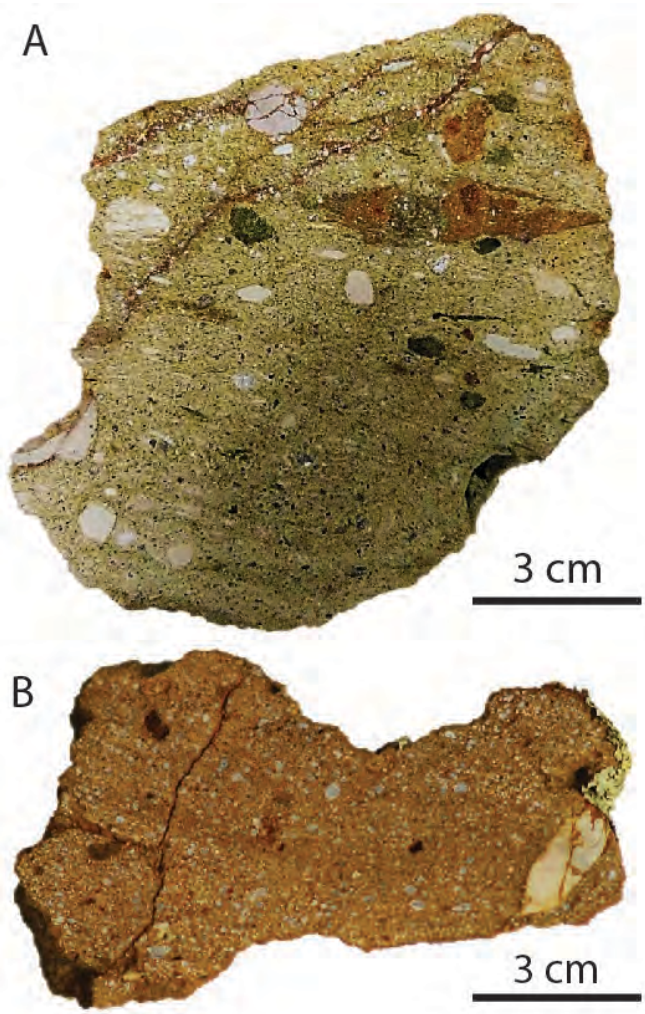

Figure 4

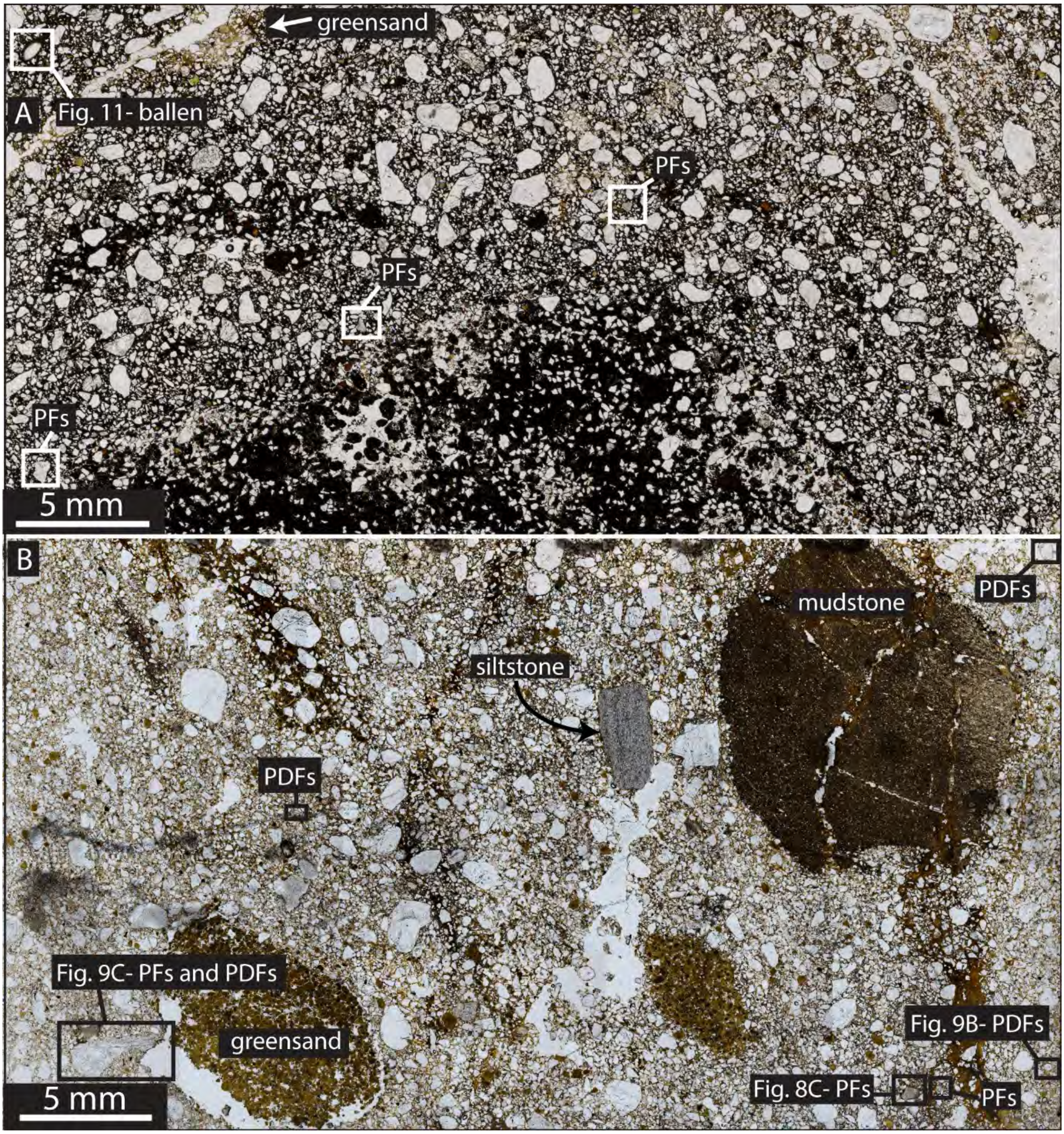

greensand
A
Fig. 11- ballen
PFs
PFs
PFs
5 mm
B
PDFs
mudstone
siltstone
PDFs
Fig. 9C- PFs and PDFs
greensand
Fig. 9B- PDFs
Fig. 8C- PFs
PFs
5 mm

Figure 5

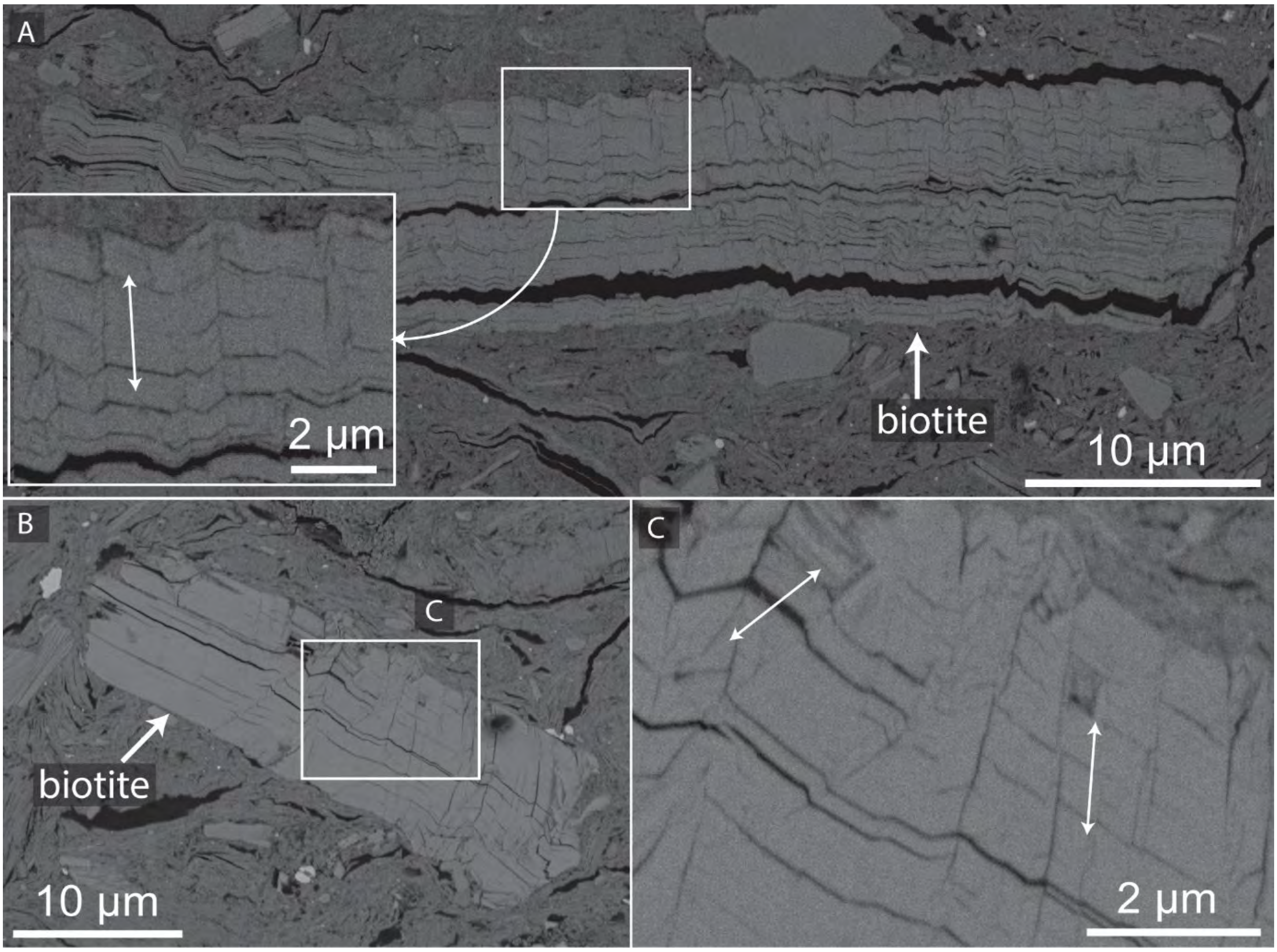

Figure 6

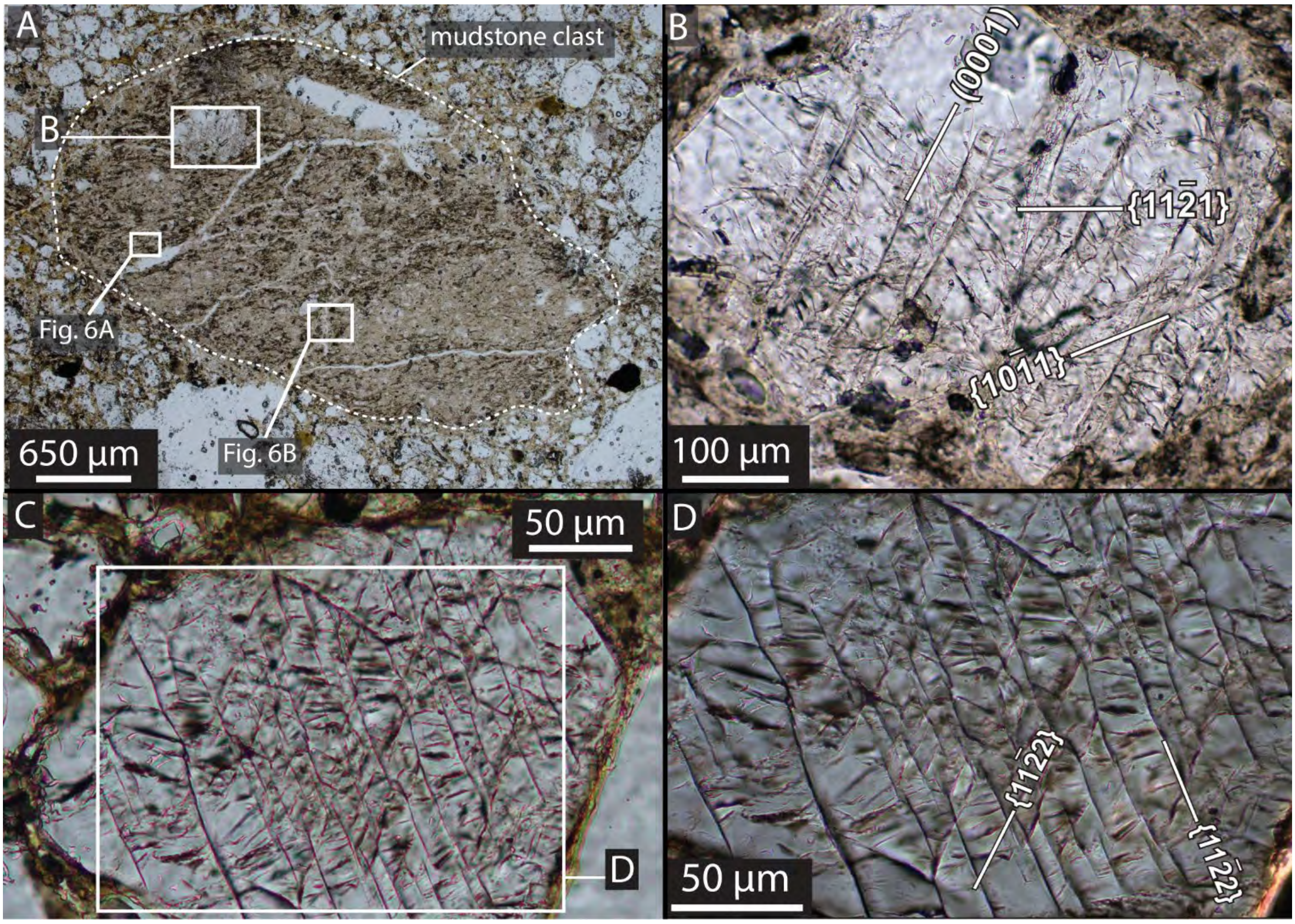
A
mudstone clast
B
Fig. 6A
Fig. 6B
650 µm
B
(0001)
{11$\bar{2}$1}
{10$\bar{1}$1}
100 µm
C
50 µm
D
D
{11$\bar{2}$2}
{11$\bar{2}$2}
50 µm

Figure 7

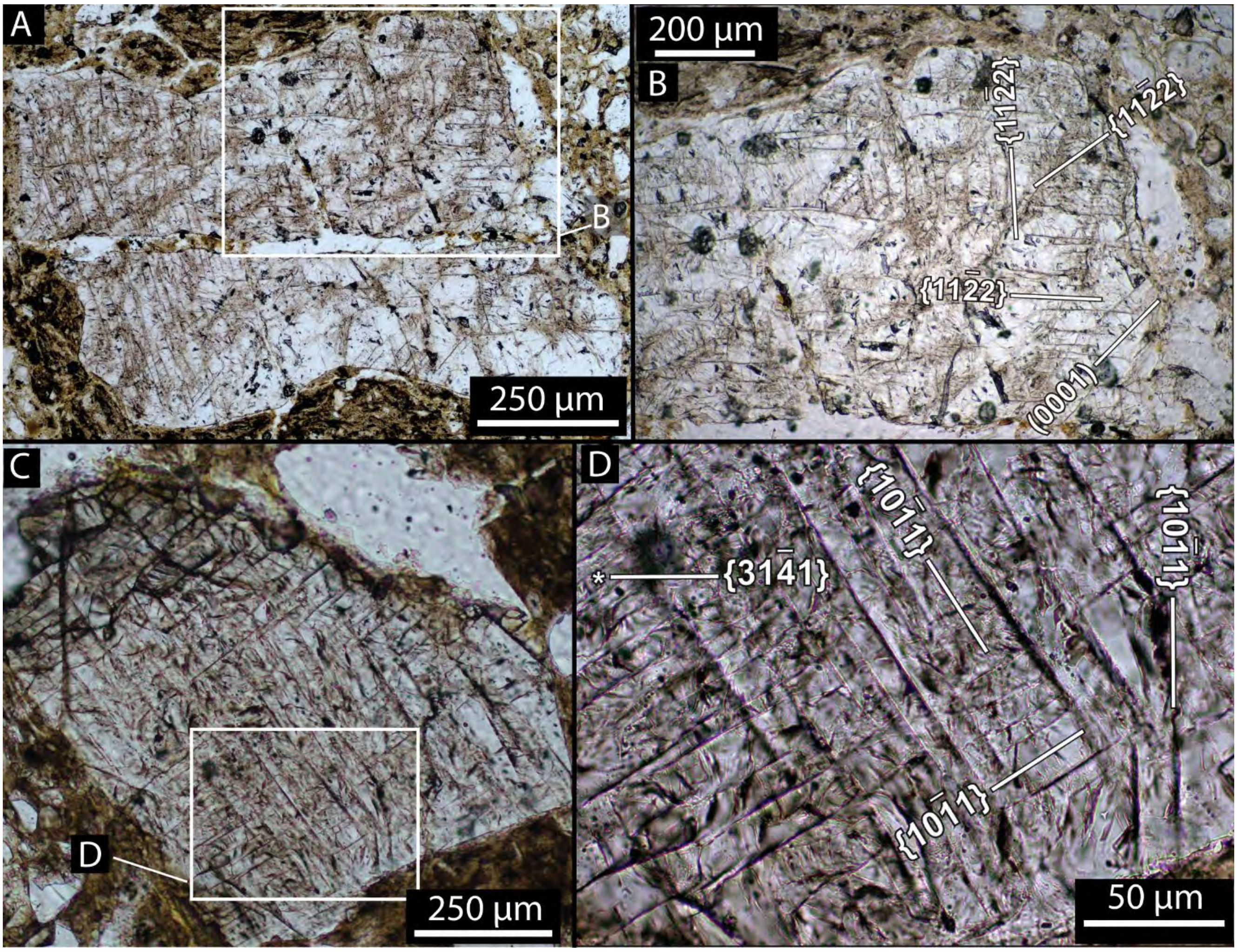
A
B
250 µm
200 µm
B
{11$\bar{2}$2}
{11$\bar{2}$2}
{11$\bar{2}$2}
(0001)
C
D
250 µm
D
*
{31$\bar{4}$1}
{10$\bar{1}$1}
{10$\bar{1}$1}
{10$\bar{1}$1}
50 µm

Figure 8

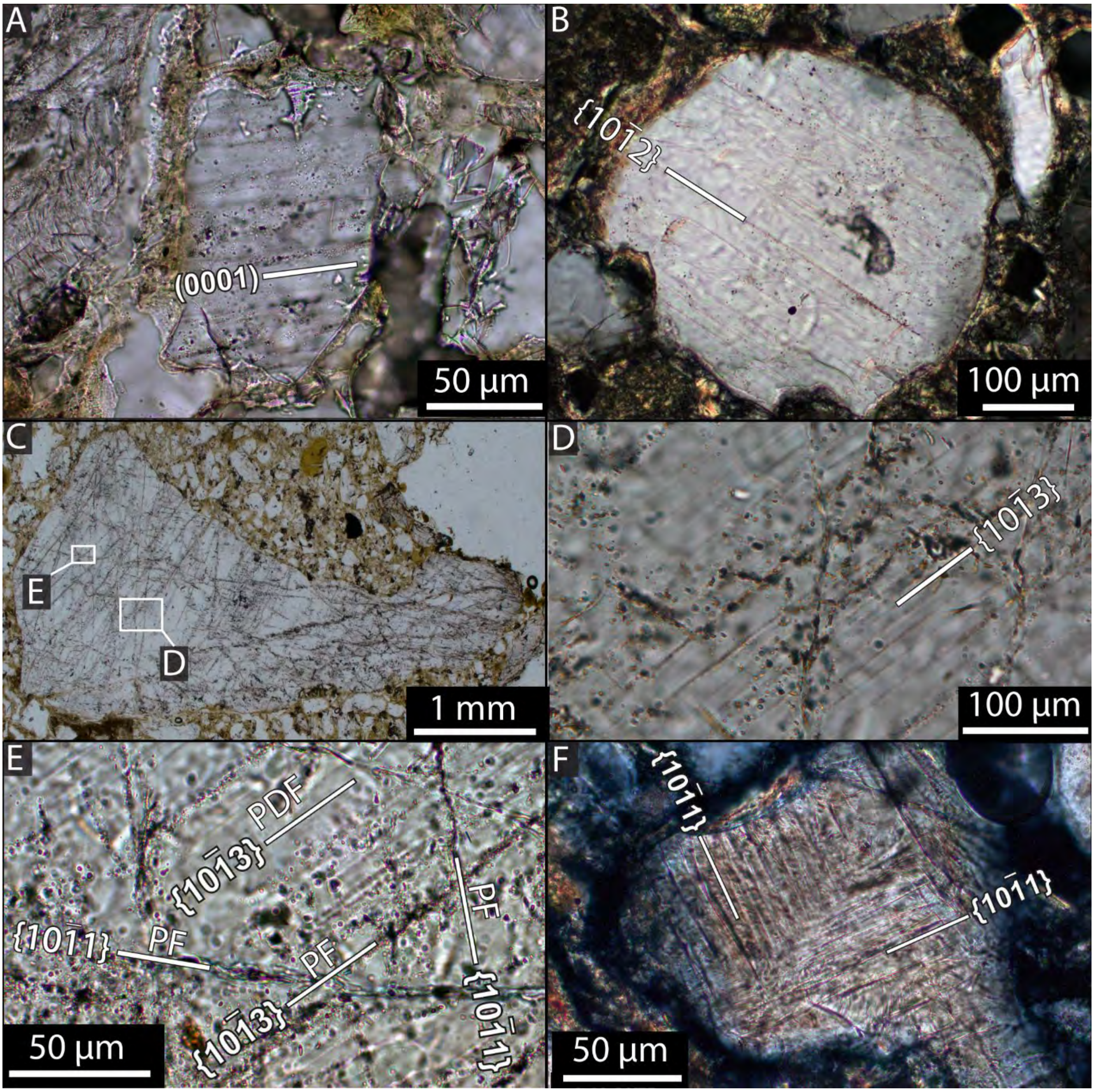
A
(0001)
50 µm
B
{10$\bar{1}$2}
100 µm
C
E
D
1 mm
D
{10$\bar{1}$3}
100 µm
E
PDF
{10$\bar{1}$3}
PF
{10$\bar{1}$1}
PF
{10$\bar{1}$3}
PF
{10$\bar{1}$1}
50 µm
F
{10$\bar{1}$1}
{10$\bar{1}$1}
50 µm

Figure 9

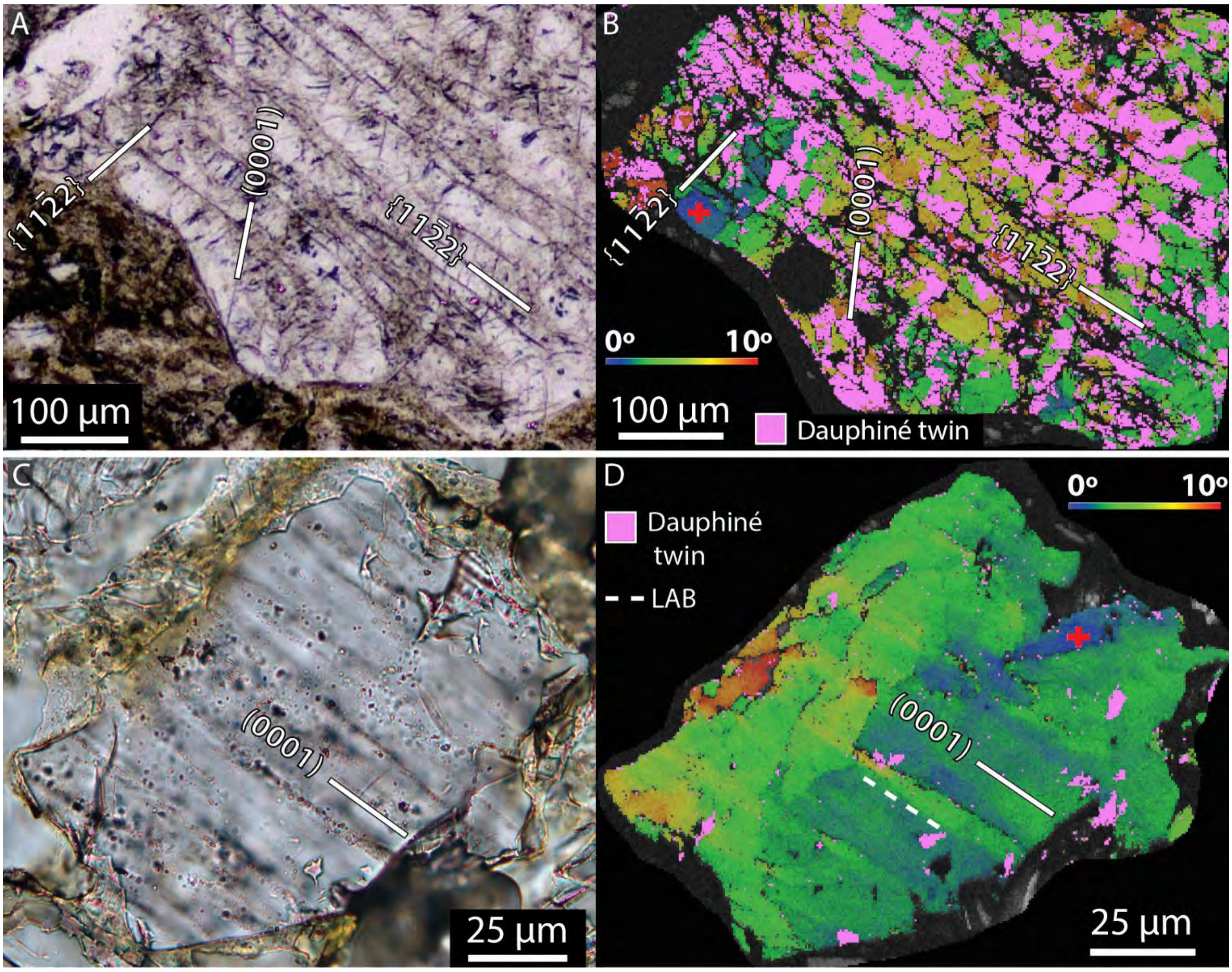
A
{11$\bar{2}$2}
(0001)
{11$\bar{2}$2}
100 µm
B
{11$\bar{2}$2}
(0001)
{11$\bar{2}$2}
0º
10º
100 µm
Dauphiné twin
C
(0001)
25 µm
D
Dauphiné twin
LAB
0º
10º
(0001)
25 µm

Figure 10

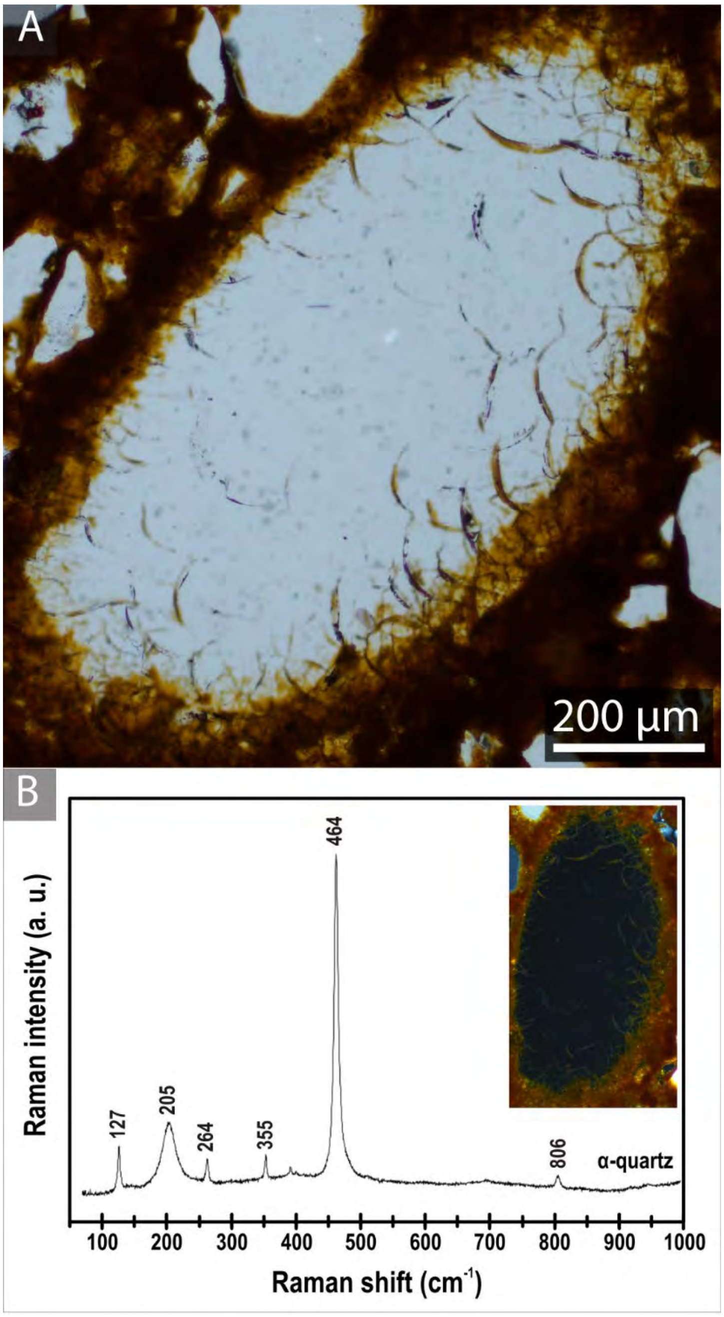
A
200 µm
B
Raman intensity (a. u.)
464
127
205
264
355
806
α-quartz
100
200
300
400
500
600
700
800
900
1000
Raman shift (cm-1)

Figure 11

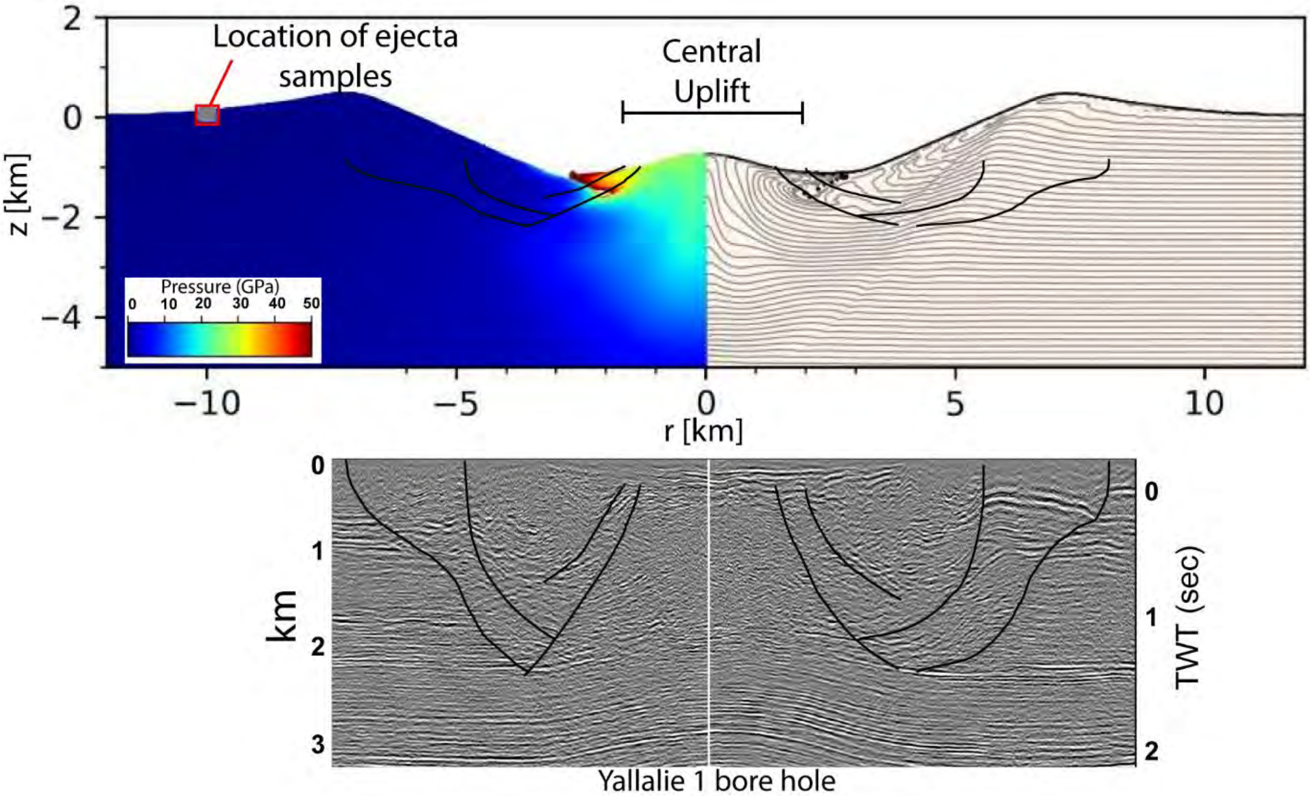
Location of ejecta
samples
Central
Uplift
z [km]
r [km]
Pressure (GPa)
0 10 20 30 40 50
2
0
−2
−4
−10
−5
0
5
10
km
TWT (sec)
Yallalie 1 bore hole

Figure 12